Supplementary Information for

Optically-Controlled Nano-Transducers Based on Cleaved Superlattices for Monitoring Gigahertz Surface Acoustic Vibrations

Changxiu Li[1], Nikolay Chigarev[1], Théo Thréard[1], Kedong Zhang[2], Nicolas Delorme[3], Vincent Tournat[1], Samuel Raetz[1], Hong Lu[2], Vitalyi E. Gusev[1,]*

[1]Laboratoire d'Acoustique de l'Université du Mans (LAUM), UMR 6613, Institut d'Acoustique – Graduate School (IA-GS), CNRS, Le Mans Université, Le Mans, France

[2]College of Engineering and Applied Sciences, Nanjing University, Nanjing, China

[3]Institut des Molécules et Matériaux du Mans (IMMM), UMR 6283 CNRS, Le Mans Université, Le Mans, France

* vitali.goussev@univ-lemans.fr

Supplementary 1

Structure of generalized Rayleigh-type surface acoustic wave on a superlattice stratified normal to its surface

The mathematical formalism for the theoretical investigation of the surface acoustic waves (SAWs) which propagate in the direction of the superlattice (SL) stratification along mechanically free surface which is normal to SL layers (Fig. S1) was developed nearly 40 years ago [S1]. In Fig. S1 a bilayer SL with individual semi-infinite plane layers oriented parallel to x_1 axis is schematically presented. In general, the layers are of different thicknesses $d^{(1)}$ and $d^{(2)}$ and are of materials with different densities $\rho^{(1,2)}$ and elastic moduli tensors $C^{(1,2)}_{\alpha\beta\gamma\delta}$.

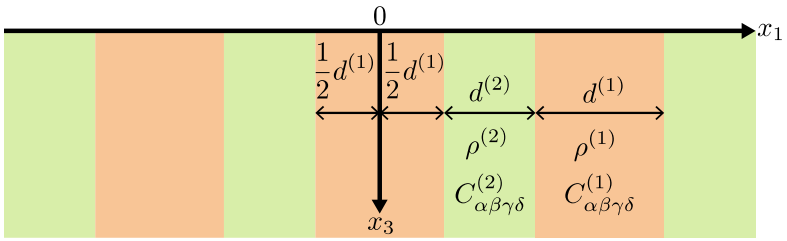

Fig. S1. Scheme of a bilayer superlattice stratified normal to the mechanically free surface.

In the geometry presented in Fig. S1 the generalized Rayleigh-type SAWs, which are denoted in the main text of the manuscript as gR waves, are polarized in the sagittal plane (x_1,x_3). In an acoustic wave of cyclic frequency ω two particle displacements components $u_\alpha(\vec{x},t) = u_\alpha(\vec{x})e^{-i\omega t}$, where ($\alpha$ = 1,3), satisfy the system of two coupled Helmholtz equations $-\omega^2\rho(\vec{x})u_\alpha = \frac{\partial}{\partial x_\beta}\left[C_{\alpha\beta\gamma\delta}(\vec{x})\frac{\partial u_\gamma}{\partial x_\delta}\right]$. Note, that the density and the elastic moduli in these equations are periodic functions of x_1 coordinate and are independent of two other coordinates. In [S1] the Helmholtz equations were specified for the case where the materials composing the SL are both of cubic symmetry, with crystallographic axes oriented along the coordinate axes in Fig. S1:

$$-\omega^2\rho(x_1)u_1(\vec{x}) = \frac{\partial C_{11}(x_1)}{\partial x_1}\frac{\partial u_1}{\partial x_1} + \frac{\partial C_{12}(x_1)}{\partial x_1}\frac{\partial u_3}{\partial x_3} + [C_{12}(x_1) + C_{44}(x_1)]\frac{\partial^2 u_3}{\partial x_1\,\partial x_3} + C_{11}(x_1)\frac{\partial^2 u_1}{\partial x_1^2} + C_{44}(x_1)\frac{\partial^2 u_1}{\partial x_3^2},$$

$$-\omega^2\rho(x_1)u_3(\vec{x}) = \frac{\partial C_{44}(x_1)}{\partial x_1}\frac{\partial u_1}{\partial x_3} + \frac{\partial C_{44}(x_1)}{\partial x_1}\frac{\partial u_3}{\partial x_1} + [C_{12}(x_1) + C_{44}(x_1)]\frac{\partial^2 u_1}{\partial x_1\,\partial x_3} + C_{11}(x_1)\frac{\partial^2 u_3}{\partial x_3^2} + C_{44}(x_1)\frac{\partial^2 u_3}{\partial x_1^2}.$$

The boundary conditions at stress-free surface x_3=0 are:

$$\left[C_{44}(x_1)\left(\frac{\partial u_1}{\partial x_3} + \frac{\partial u_3}{\partial x_1}\right)\right]_{x_3=0} = 0, \qquad \left[C_{12}(x_1)\frac{\partial u_1}{\partial x_1} + C_{11}(x_1)\frac{\partial u_3}{\partial x_3}\right]_{x_3=0} = 0.$$

These equations and boundary conditions are valid for all the SLs in our experiments. In [S1] the mathematical formalism for revealing the gR SAWs was developed for an arbitrary periodic distributions of density $\rho(x_1)$ and elastic moduli $C_{11}(x_1), C_{12}(x_1)$ and $C_{44}(x_1)$, expanding them in the Fourier series:

$$f(x_1) = \sum_{m=-\infty}^{\infty} f(m)e^{imqx_1},\ f(m) = \frac{1}{d_{SL}}\int_{-d_{SL}/2}^{d_{SL}/2} dx_1\, f(x_1)e^{-imqx_1}, \qquad \text{(S1)}$$

where f denotes either the density or the elastic modulus, $d_{SL} \equiv d^{(1)} + d^{(2)}$ and $q_{SL} \equiv 2\pi/d_{SL}$

are the SL period and SL wave number, respectively. In accordance with Bloch-Floquet property of the waves in the spatially periodic media [S2] the solution of the Helmholtz equations for the bulk eigen modes has the following form:

$$u_\alpha(x_1, x_3) = \sum_{m=-\infty}^{\infty} u_\alpha(m, x_3) e^{ik_m x_1}, \quad \text{(S2)}$$

where $k_m = k + q_{SL}m$. Thus, each component of the mechanical displacement is a periodic function along x_1 axis composed of the component with wave number k, corresponding to $m = 0$ in Eq. (S2) and independent of the SL periodicity, and an infinite number of the components with wave numbers shifted relative to k by a $q_{SL}m$ ($m = \pm 1, \pm 2, \ldots.$). Saying differently, each component $u_\alpha(x_1, x_3)$ of the mechanical displacement vector is composed of an infinite number of contributions from all the « diffraction orders » m. The periodic inhomogeneity of the material couples all the « diffraction orders » and it also couples different components of the mechanical displacement additionally to their coupling by the boundary conditions. Substitution of the spatially periodic distributions of the material parameters, Eq. (S1), and of the mechanical displacements, Eq. (S2), in the system of the Helmholtz equations results in the infinite system of coupled algebraic equations for $u_\alpha(m, x_3)$ [S1]. For the particular frequencies ω, the evanescent bulk eigen modes, i.e., those decaying with the increasing distance x_3 from the surface (x_1,x_2), can be combined with particular relative amplitudes to satisfy the conditions at the stress-free surface. In [S1] an infinite system of equations for the amplitudes of the bulk components contributing to the surface acoustic wave was derived. These equations are compatible only for the particular values of frequencies, which are the eigen frequencies of the SAWs. Because all the wave numbers $k_m = k + qm$ of the displacement field are equivalent, the dispersion relations $\omega = \omega(k)$ of the acoustic waves in the structure presented in Fig. S1 can be folded inside the Brillouin zone $-\pi/d_{SL} \leq k \leq \pi/d_{SL}$, where $\pi/d_{SL} \equiv k_{edge}$ denotes the Brillouin zone edge (Fig. S2 and Fig. 2 (c) of the manuscript).

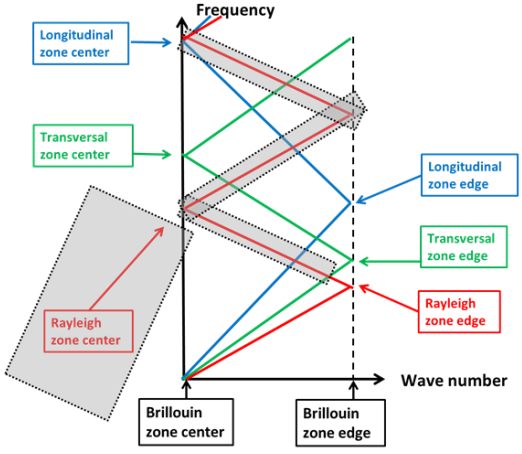

Figure S2. Schematic presentation of the surface Rayleigh modes (red lines) and surface skimming transverse and longitudinal bulk modes (green and blue lines, respectively) in the Brillouin zone, obtained by formal folding the dispersion relations of the surface and bulk modes in an "average" homogenous medium. The lowest (acoustical-type) branches of the surface skimming bulk waves describe the boundaries for the existence of the bulk modes. The Rayleigh SAW $\omega(k = 0) = \omega_R$ obtained in the limit $\mu = 0$ is marked as Rayleigh zone center mode. In the limit $\mu \neq 0, \mu \ll 1$, the SAW weakly interacts with the bulk acoustic modes. The parts of the SAW spectrum that are expected to be modified by these interactions are symbolically shaded in grey. The developed theory predicts that this interaction results in small shift of the frequency and in weak attenuation of the gR wave in the Brillouin zone center, i.e., $\Delta Re(\omega_R)/\omega_R \sim \mu^2, Im(\omega_R)/\omega_R \sim \mu^2$. The revealed gR wave in the limit $\mu \neq 0, \mu \ll 1$ is, in general, a three-component wave, while in the limit $\mu = 0$ it is a two-component wave. Additionally, $\mu \neq 0$ generally results in frequencies splitting of symmetrical and anti-symmetrical gR waves in the center and the edge of the Brillouin zone (not presented in the scheme, but evidenced in Fig. 2 (c) of the manuscript).

The derived systems of algebraic equations were solved in [S1] only numerically and only non-attenuated SAWs, i.e., with real valued frequencies, were in the scope of [S1]. Thus, mostly the lowest (acoustical-type) branch of the SAW dispersion relation was evaluated from the zone center, where for this mode $\omega(k = 0) = 0$, to the zone edge $k = k_{edge}$. The possibility of the gap opening between acoustical-type SAW branch and the nearest in frequencies (first) optical-type SAW branch at the Brillouin zone edge was revealed. The first optical-type SAW branch was studied in [S1] only rather close to the zone edge. With the diminishing wave number, the first optical-type SAW branch intersects the lowest (acoustical-type) branches of the bulk modes, e.g. Fig. S2 and Fig. 2 (c) of the manuscript. At wave numbers smaller than the first intersection point, the SAW is supersonic relative to some of the bulk modes and emits energy in the bulk of the sample. Purely real solution for the SAW eigen frequency disappears. The attenuated SAWs, including optical-type SAW modes in the zone center ($k = 0$) and nearby, which are playing the dominant role in our experiments, were not studied in [S1] at all.

In our experiments, the k spectrum of the photo-generated SAWs is controlled by the spatial distribution of the stresses that could be photo-induced by the pump laser pulses. Of course, in general, the distribution of the photo-induced stresses depends on the physical mechanisms of optoacoustic conversion (thermoelasticity, electron-phonon deformation potential, inverse piezoelectric effect, electrostriction, etc. [S3, S4]). The dominant physical mechanisms in each particular case are determined by the physical properties of the materials composing the SL and the energy quanta of the pump laser radiation. For example, the pump light penetration depth in the materials composing the SL can importantly influence the depth distribution of the photo-induced stresses [S3, S4]. The universal influence on the lateral distribution of the photo-induced stresses, i.e., along the free surface, and, respectively, on the k spectrum of the photo-induced stresses, stems from the lateral distribution of the pump laser radiation penetrating inside the SL. In our experiments, the lateral modulation of the photo-induced stresses at nanometer spatial scales is due to the difference in the optical properties of the two layers. In the infinite SL composed of spatially homogeneous layers the stresses photo-induced by the laterally homogeneous incident pump laser radiation will have the periodicity of SL and will exhibit the Bloch-Floquet property. Thus, in this limiting case the folded k spectrum of the photo-induced stresses would contain only zone center components, $k = 0$. Focusing of the pump laser radiation localizes initial optical excitation laterally at the scale which is larger or comparable to the pump optical wavelength. Consequently, in our experiments the k spectrum of the photo-induced stresses would be broadened. However, in our experiments, the period of the SL, d, is much smaller than the optical wavelengths. Therefore, this broadening is much narrower than the width of the Brillouin zone $\pi/d_{SL} \equiv k_{edge}$. Consequently, the photo-generated SAWs k spectrum is expected to be strongly localized near the Brillouin zone center $k = 0$.

In order to get a physical insight relevant to our experiments, we drastically simplified the general approach for the description of the gR waves [S1]. Firstly, based on the above-described arguments, we evaluate analytically only $k = 0$ modes. Secondly, assuming the layers of equal thickness, we take into account only the first two lowest order components of the waves, i.e., corresponding to $m = 0$ and $m = \pm 1$, in Eq. (S2). This simplification is based on the following arguments. If $d^{(1)} = d^{(2)}$, then only $m = 0$ and odd m contribute to the Fourier spectra of the material parameter distributions in Eq. (S1), while the Fourier components with $|m| > 1$ are significantly smaller than $|m| = 1$ components. The same is valid for the lateral components of the pump laser intensity penetrating inside the infinite SL because they are controlled by the periodic distribution of optical reflection

coefficient. Consequently, the dominant components in the SAWs are expected to be $m = 0$ and $|m| = 1$, coupled inside the SL by the Fourier components $|m| = 1$ of the density and of the elastic moduli distributions. Thirdly, as the laser spot size on focal plane is much larger than the SL period, the lateral variations of the photo-induced stresses across an individual layer thickness are small in comparison with the stresses themselves. This leads to the expectations that the symmetric motions of the individual SL layers are photo-excited with larger amplitudes than antisymmetric ones. A symmetric mode exhibits, relative to the central plane of the individual layer, an odd distribution of the horizontal mechanical displacement, u_1, and an even distribution of vertical mechanical displacement, u_3. Combining the above assumptions, we search the solutions of the Helmholtz equations for the bulk modes in the following simplified form:

$$u_1(x_1, x_3) = 2u_S\, sin(q_{SL}x_1)e^{-\alpha x_3}, u_3(x_1, x_3) = [u_0 + 2u_C cos(q_{SL}x_1)\,]e^{-\alpha x_3},$$

$$\boldsymbol{f}(x_1) = \langle f\rangle + 2\Delta f\cos(q_{SL}), \langle f\rangle = \left(f^{(1)} + f^{(2)}\right)/2, \Delta f = \left(f^{(1)} - f^{(2)}\right)/\pi. \quad \text{(S3)}$$

Here α denotes the depth propagation/penetration constant [S1], related to the projection of the acoustic wave vector on the x_3 direction. Substitution of the displacement field (S3) and the spatial distributions of density $\rho(x_1)$ and elastic moduli $C_{11}(x_1), C_{12}(x_1)$ and $C_{44}(x_1)$ in the Helmholtz equations and separation of the constant terms and the terms proportional to $sin(qx_1)$ and to $cos(qx_1)$, results in the system of equations for the displacement amplitudes u_S, u_0 and u_c:

$$\begin{pmatrix} [\omega^2\rho + \alpha^2 C_{44} - q_{SL}^2 C_{11}] & \alpha q_{SL}(C_{12} + C_{44}) & \alpha q_{SL}\Delta C_{12} \\ -\alpha q_{SL}(C_{12} + C_{44}) & [\omega^2\rho + \alpha^2 C_{11} - q_{SL}^2 C_{44}] & [\omega^2\Delta\rho + \alpha^2\Delta C_{11}] \\ -\alpha q_{SL}\Delta C_{12} & [\omega^2\Delta\rho + \alpha^2\Delta C_{11}] & \frac{1}{2}[\omega^2\rho + \alpha^2 C_{11}] \end{pmatrix}\begin{pmatrix} u_S \\ u_C \\ u_0 \end{pmatrix} = \begin{pmatrix} 0 \\ 0 \\ 0 \end{pmatrix}.$$

The compatibility condition for these equations defines the bulk eigen modes in the geometry presented in Fig. S1. Although the compatibility condition can be solved exactly, we use here the method of the successive approximations, based on the following assumption of a weak modulation of the material parameters: $\Delta\rho/\langle\rho\rangle \sim \Delta C_{12}/\langle C_{12}\rangle \sim \Delta C_{11}/\langle C_{11}\rangle \sim \mu \ll 1$. This inequality is satisfied sufficiently well in our samples and leads to very insightful estimates. Additionally, to avoid rather cumbersome formulas and get even more insightful predictions, we assume that the SL is composed of elastically isotropic layers, $C_{12} = C_{11} - 2C_{44}$. Therefore, relations between the elastic moduli and the velocities of the bulk acoustic waves are significantly more compact than in the cubic crystals: $C_{11} = \rho C_L^2$ and $C_{44} = \rho C_T^2$. Here C_L and C_T denote the velocities of the longitudinal and the transverse bulk acoustic waves, respectively. The equations for the eigen modes take the from:

$$\begin{pmatrix} \left[\omega^2 + \alpha^2 C_T^2 - q_{SL}^2 C_L^2\right] & \alpha q_{SL}(C_L^2 - C_T^2) & \sim\mu \\ -\alpha q_{SL}(C_L^2 - C_T^2) & \left[\omega^2 + \alpha^2 C_L^2 - q_{SL}^2 C_T^2\right] & \sim\mu \\ \sim\mu & \sim\mu & \frac{1}{2}[\omega^2 + \alpha^2 C_L^2] \end{pmatrix}\begin{pmatrix} u_S \\ u_C \\ u_0 \end{pmatrix} = \begin{pmatrix} 0 \\ 0 \\ 0 \end{pmatrix}, \quad \text{(S4)}$$

where the small parameter μ is defined as $\mu \sim \Delta\rho/\langle\rho\rangle \sim \Delta C_L/\langle C_L\rangle \sim \Delta C_T/\langle C_T\rangle \ll 1$. In the limit of infinitely small, i.e., disappearing, modulation of the sample parameters, we assume $\mu = 0$. Then, the compatibility condition for Eq. (S4) predicts three bulk acoustic modes differing by their depth propagation constants $\alpha_{z,L,T}$: laterally unmodulated bulk longitudinal $k = 0$ mode ($\alpha_Z^2 = -(\omega/C_L)^2 \equiv -k_L^2$), laterally modulated bulk longitudinal $k = 0$ mode ($\alpha_L^2 = q_{SL}^2 - (\omega/C_L)^2 \equiv q_{SL}^2 - k_L^2$) and laterally modulated bulk transversal $k = 0$ mode ($\alpha_T^2 = q_{SL}^2 - (\omega/C_T)^2 \equiv q_{SL}^2 - k_T^2$). Saying differently, the theory predicts a single wave (longitudinal) in the zeroth diffraction order ($m = 0$) and two waves (longitudinal and transverse) in the first diffraction orders ($m = \pm 1$). Note that the

transverse acoustic mode is absent in the zeroth diffraction order via symmetry considerations, because we have limited our analysis to the symmetric modes only. In the presence of a weak modulation of the material parameters in the SL, $\mu \ll 1 \neq 0$, the revealed three modes become coupled because of the scattering on the SL spatial periodicity. However, this scattering leads only to small modifications of the depth propagation constants, i.e., $\sim\mu^2$: $\alpha_{z,L,T} \Rightarrow \alpha_{z,L,T}\left(1-\beta_{z,L,T}\mu^2\right) \equiv \alpha_{z,L,T}^{(\mu)}$. Here $\beta_{z,L,T}$ is of the order μ^0.

Each of the above-derived eigen modes includes the components u_S, u_c and u_0 (in a particular proportions), and, as a consequence, the components of the mechanical displacement include, in general, the contributions from all three eigen modes:

$$u_1 = \sum_{j=z,L,T} 2A_j \, sin(q_{SL}) e^{-\alpha_j^{(\mu)} x_3},\; u_3 = \sum_{j=z,L,T} A_j \left[\left(\frac{u_0}{u_S}\right)_j + 2\left(\frac{u_C}{u_S}\right)_j cos(q_{SL}x_1) \right] e^{-\alpha_j^{(\mu)} x_3}. \quad \text{(S5)}$$

In the considered case of the weak modulation, $\mu \ll 1$, the proportions of the different components in the displacements structure are controlled in the leading order by the following relations: $\left(\frac{u_C}{u_S}\right)_{z,L,T} \sim\mu^0, \left(\frac{u_0}{u_S}\right)_{L,T} \sim\mu, \left(\frac{u_0}{u_S}\right)_{z} \sim\mu^{-1}$. The choice of the amplitudes A_j in the displacement fields (S5) provides opportunity to satisfy the boundary conditions at mechanically free surface. Substitution of the displacement fields (S5) and the spatial distributions of the elastic moduli $C_{11}(x_1), C_{12}(x_1)$ and $C_{44}(x_1)$ in the boundary conditions and separation of the constant terms and the terms proportional to $sin(q_{SL}x_1)$ and to $cos(q_{SL}x_1)$, results in the system of equations for the displacement amplitudes A_z, A_L and A_T:

$$\begin{pmatrix} \gamma_{11}+\delta_{11}\mu^2 & \gamma_{12}+\delta_{12}\mu^2 & \gamma_{13}+\delta_{13}\mu^2 \\ \gamma_{21}+\delta_{21}\mu^2 & \gamma_{22}+\delta_{22}\mu^2 & \gamma_{23}+\delta_{23}\mu^2 \\ \gamma_{31}\mu & \gamma_{32}\mu & \gamma_{33}\mu^{-1}+\delta_{33}\mu \end{pmatrix} \begin{pmatrix} A_L \\ A_T \\ A_z \end{pmatrix} = \begin{pmatrix} 0 \\ 0 \\ 0 \end{pmatrix}. \quad \text{(S6)}$$

In Eq. (S6) γ_{ij} and δ_{ij} are the constants of the μ^0 order, and only the terms of the first two leading orders are kept in each of the equations composing the system (S6). In accordance with (S6), when μ=0, the laterally unmodulated mode, i.e., z mode, does not contribute to the SAW (A_z=0), while the modes A_L and A_T are coupled via: $\begin{pmatrix} \gamma_{11} & \gamma_{12} \\ \gamma_{21} & \gamma_{22} \end{pmatrix} \begin{pmatrix} A_L \\ A_T \end{pmatrix} = \begin{pmatrix} 0 \\ 0 \end{pmatrix}$. Here the matrix $\begin{pmatrix} \gamma_{11} & \gamma_{12} \\ \gamma_{21} & \gamma_{22} \end{pmatrix}$ is proportional to the Rayleigh SAW matrix $\begin{pmatrix} 2\alpha_L & \alpha_T + q^2/\alpha_T \\ (c_L^2 - 2c_T^2)q_{SL} - c_L^2\alpha_L^2/q_{SL} & -2c_T^2 q_{SL} \end{pmatrix}$. The Rayleigh determinant is zero, $\left(2q_{SL}^2 - k_T^2\right)^2 - 4q_{SL}^2\alpha_L\alpha_T = 0$, at the frequencies ω_R of the Rayleigh SAW eigenmode. This solution, obtained in the limit $\mu = 0$, predicts that the gR wave at $\omega = \omega_R$ with the propagation vector equal to $k = q_{SL} \equiv 2\pi/d_{SL}$, i.e., with the initially expected periodicity, belongs in the scheme of folded Brillouin zone to the optical-type branch of the gR wave, $\omega(k = 0) = \omega_R$ (Fig. S2). It propagates at the Rayleigh velocity c_R of an « average » medium.

When $\mu \neq 0$ all three amplitudes of the bulk modes A_L, A_T and A_z in Eq. (S5) are coupled in the gR wave, which contains a laterally unmodulated part, although smaller than the modulated ones:

$$u_1 \sim \mu^0 sin(q_{SL}x_1), u_3 \sim \mu + \mu^0 \, cos(q_{SL}x_1). \quad \text{(S7)}$$

Equation (S7) describes the lateral structure of the horizontal and vertical components of the mechanical displacement on the free surface. The complete description of the spatial structure of the generalized Rayleigh SAWs in the limit $\mu \neq 0, \mu \ll 1$ could be obtained from Eq. (S6), which predicts that in this limit $A_z \sim \mu^2 A_L \sim \mu^2 A_T$. Therefore, if the corrections $\sim\mu^2$ are omitted, in the

description of the gR wave, the spatial structure of the generalized Rayleigh wave can be described by

$$u_1 = \sum_{j=L,T} 2A_j \, sin(q_{SL}x_1)e^{-\alpha_j x_3}, u_3 = \sum_{j=L,T} A_j \left[\left(\frac{u_0}{u_S}\right)_j + 2\left(\frac{u_C}{u_S}\right)_j cos(q_{SL}x_1) \right] e^{-\alpha_j x_3}, \quad \text{(S8)}$$

where the ratio of A_L and A_T can be evaluated in the limit $\mu = 0$. Thus, if the corrections $\sim\mu^2$ are omitted, then the generalized Rayleigh wave is a two-component wave similar to the Rayleigh wave in the limit $\mu = 0$, however the two evanescent bulk components (modes) of the gR wave contain, in comparison with the Rayleigh wave in averaged medium, the laterally unmodulated contributions, i.e., Eq. (S8). In comparison with the frequency of the Rayleigh wave predicted in the absence of the parameters modulation, $\omega_R = q_{SL}c_R = 2\pi c_R/q_{SL}$, the frequency evaluated with parameters modulation shifts by $\Delta Re(\omega_R)/\omega_R \sim \mu^2$ and it acquires an imaginary part $Im(\omega_R)/\omega_R \sim \mu^2$.

The above-presented simplest theory, predicts that surface confined modes on a semi-infinite SL stratified normal to its surface contain laterally homogeneous components in their mode structure. This means that, potentially, these modes could be excited even by a laterally homogeneous (averaged over the SL period) part of the distributed photo-induced stresses and even in the case of a SL without any optical contrast between the layers. This also suggests that they could be detected by normally incident probe radiation as oscillating motion of the laterally homogeneous (averaged over the SL period) near-surface layer of the sample. Importantly, in the case of weak modulation of the materials parameters in the SL, these generalized Rayleigh-type SAWs exhibit weak attenuation.

[S1] Djafari-Rouhani, B., Maradudin, A. A., & Wallis, R. F. (1984). Rayleigh waves on a superlattice stratified normal to the surface. *Physical Review B*, *29*(12), 6454.

[S2] Kittel, C., McEuen, P., & McEuen, P. (1996). *Introduction to solid state physics* (Vol. 8, pp. 105-130). New York: Wiley.

[S3] Akhmanov, S. A., & Gusev, V. É. (1992). Laser excitation of ultrashort acoustic pulses: New possibilities in solid-state spectroscopy, diagnostics of fast processes, and nonlinear acoustics. *Soviet Physics Uspekhi*, *35*(3), 153.

[S4] V. Gusev and A. Karabutov, Laser Optoacoustics (AIP, New York, 1993).

Supplementary 2

Optical detection of generalized Rayleigh-type surface acoustic wave on a superlattice stratified normal to its surface

In picosecond laser ultrasonics, the acoustic waves in the GHz-THz frequency range are detected via the interference on the photodetector of the probe light scattered by them and the probe light scattered by the stationary surfaces/interfaces of the sample. The general approach to predict the transient acoustically induced optical reflectivity changes, monitored by the photodetector, consists of the three following stages. Firstly, the probe light fields reflected by the sample and transmitted into the sample in the absence of the coherent acoustic waves should be evaluated. The probe light reflected by the sample and incident on the photodetector should be predicted. Secondly, the probe light scattered by the acoustic wave either at the sample surface or in the bulk of the sample, or both should be evaluated. The scattered light reaching the photodetector should be predicted. Thirdly, the component of the probe light intensity incident on the photodetector, which is proportional to the product of the amplitudes of the reflected and scattered light should be found. The components of the intensity, which depend only on the intensity of the reflected light, do not provide information on the acoustic waves, while the intensity components which depend only on the intensity of the acoustically scattered light are negligibly small, because of the small amplitude of the acoustically-scattered probe light, in comparison with the amplitudes of the reflected probe light.

To get insightful predictions on the detection of the generalized Rayleigh-type SAWs, which are denoted in the main text of the manuscript as gR waves, in the SL presented in Figs. S1 and S3, we retain all the simplifying assumptions predicting the gR SAWs, leading to their description in Eq. S8, and we introduce both specific and similar simplifying assumptions for the description of the probe light field.

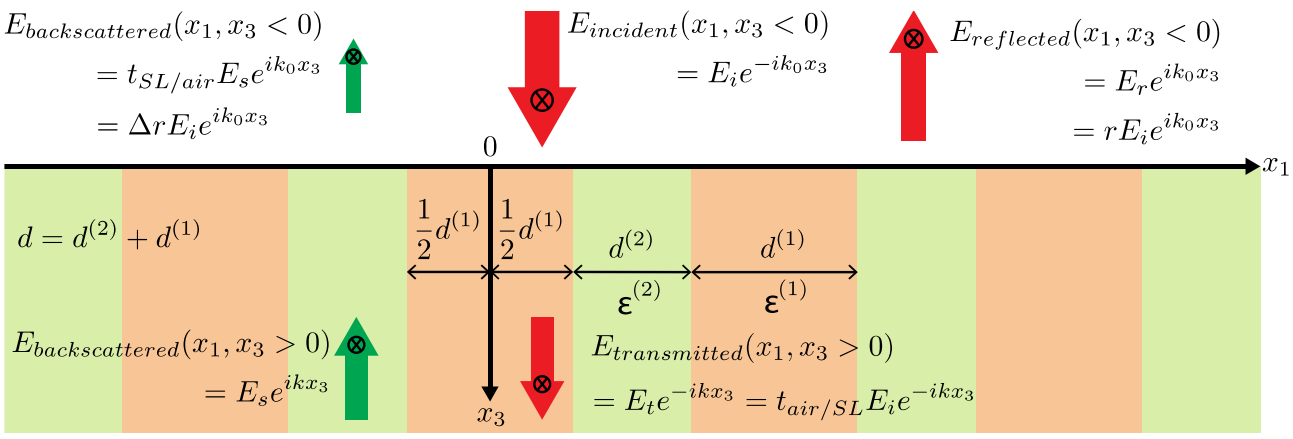

Figure S3. Schematic presentation of the Brillouin scattering of probe light by the gR SAW in the SL stratified normal to the mechanically free surface. In the considered case of sub-optical SL, only plane laterally unmodulated reflected, transmitted and scattered waves should be accounted for the description of the leading order optical and acousto-optical processes. $t_{SL/air}$ and $t_{air/SL}$ denote the transmission coefficient of light from the SL into the air and in the opposite direction, respectively. The acoustically induced changes in transient optical reflectivity monitored by the photodetector result from the heterodyning at the photodetector of the acoustically backscattered probe light $\sim \Delta r E_i$ by the probe light reflected at the air/SL interface $\sim r E_i$.

The first specific assumption, which makes the problem significantly less cumbersome, while retaining the main features of the detection process, is the postulation that the normally incident probe light field is polarized parallel to the surfaces of the individual layers, i.e., in the (x_2,x_3) plane. Under this assumption, although the layered half-space under consideration is, in general, an optically anisotropic/birefringent medium [S6], the probe light incident along the optical symmetry axis, does not exhibit any mode conversion in the reflection/transmission by the SL, and can be described by a single component of the electric field, i.e., $E_{incident} = E_2 \equiv E_i$. The reflected probe light incident on the photodetector, which provides heterodyning of the acoustically scattered light, is the light polarized as the incident one. Therefore, if the probe light is mode converted in its scattering by the acoustic field, then the second process of its mode conversion would be required to allow its interference with the reflected light. This second mode conversion could be also only due to the acoustic waves. Each mode conversion introduces additional smallness in the resulting light field, because the SAWs are of small amplitude. Thus, we omit here the contributions to the transient reflectivity signal of the probe light mode conversion processes. However, it is worth noting that a modified optical scheme, i.e., of the depolarized transient reflectivity measurements, can be suggested for the dedicated study of these processes and the detection of SAWs via these processes, if required.

The probe light in the geometry of Fig. S3 is described by the following Helmholtz equation:

$$\left(\frac{\partial^2}{\partial x_1^2} + \frac{\partial^2}{\partial x_3^2}\right) E + k_0^2 \varepsilon(x_1, x_3) E = 0. \tag{S9}$$

Here k_0 is the probe wave number in vacuum, $\varepsilon(x_1, x_3 > 0)$ is the relative permittivity of the SL, while the permittivity of air is $\varepsilon(x_1, x_3 < 0) \equiv 1$. Under the assumptions identical to those leading to Eq. (S3), the distributions of the relative permittivity in the SL and the probe light eigen modes in the system presented in Fig. S3 have the following simplest descriptions

$$\boldsymbol{\varepsilon}(x_1, x_3 > 0) = \langle \varepsilon \rangle + 2\Delta\varepsilon \cos(q_{SL} x_1), \langle \varepsilon(x_3 > 0) \rangle = \frac{d^{(1)}\varepsilon^{(1)} + d^{(2)}\varepsilon^{(2)}}{d^{(1)} + d^{(2)}},$$

$$\Delta\varepsilon(x_3 > 0) = \frac{1}{\pi}\left(\varepsilon^{(1)} - \varepsilon^{(2)}\right) cos\left[\frac{\pi}{2}\frac{|d^{(1)} - d^{(2)}|}{(d^{(1)} + d^{(2)})}\right],$$

$$E(x_1, x_3) = [\langle E \rangle + 2E_C cos(q_{SL} x_1)\,] e^{-\beta x_3}. \tag{S10}$$

Here β denotes the propagation/penetration constant, related to the projection of the optical wave vector on the x_3 direction. The approximation suggested in Eq. (S10), results in the following solution of Eq. (S9) for the reflected probe light,

$$E_{reflected}(x_1, x_3 < 0) = \langle E_r \rangle\, e^{ik_0 x_3} + 2E_{r,C} cos(q_{SL} x_1) e^{i\sqrt{k_0^2 - q_{SL}^2}\, x_3}. \tag{S11}$$

Note, that the second contribution to the reflected light in Eq. (S11) is an evanescent wave for the considered-by-us sub-optical SLs, as $k_0 < q_{SL}$. Thus only the plane (laterally unmodulated) component of the reflected probe light reaches the photodetector for the interference with the acoustically scattered probe light and, consequently, only the plane components of the scattered light reaching the photodetector could contribute to the transient reflectivity signal. The substitution of Eq. (S10) into Eq. (S9) leads to the description of the optical eigen modes inside the SL

$$\begin{pmatrix} \beta^2 - q_{SL}^2 + k^2 & \left(\frac{\Delta\varepsilon}{\langle\varepsilon\rangle}\right) k^2 \\ 2\left(\frac{\Delta\varepsilon}{\langle\varepsilon\rangle}\right) k^2 & \beta^2 + k^2 \end{pmatrix} \begin{pmatrix} E_C \\ \langle E \rangle \end{pmatrix} = \begin{pmatrix} 0 \\ 0 \end{pmatrix},\ k^2 \equiv \langle\varepsilon\rangle k_0^2 \equiv n^2 k_0^2. \tag{S12}$$

Equation (S12) predicts inside the SL two optical modes with the different propagation/penetration constants,

$\beta_{\mp}^2 = -q_{SL}^2 + \frac{q_{SL}^2}{2}\left[1 \mp \sqrt{1 + 2\left(2\frac{k^2}{q_{SL}^2}\right)^2\left(\frac{\Delta\varepsilon}{\langle\varepsilon\rangle}\right)^2}\right] \equiv -k^2 + \frac{q_{SL}^2}{2}\left[1 \mp \sqrt{1+2\eta^2}\right]$. Here a compact notation η is introduced for a parameter $\eta \equiv \left(2\frac{k^2}{q_{SL}^2}\right)\left(\frac{\Delta\varepsilon}{\langle\varepsilon\rangle}\right) = \left(2\frac{d_{SL}^2}{\lambda^2}\right)\left(\frac{\Delta\varepsilon}{\langle\varepsilon\rangle}\right) << 1$, which is small in sub-optical SLs with $k^2 \ll q_{SL}^2$ even in the case of strong optical contrast between the individual SL layers, i.e., $\Delta\varepsilon \sim \langle\varepsilon\rangle$. The existence of a small parameter η is another difference in the theory of the optical detection of SAWs in comparison with the theory of the SAW eigen modes in Supplementary S1. Neglecting the corrections of the order η^2 to the propagation constants and to the modes structure in general, the transmitted and acoustically backscattered probe light fields inside the SL can be presented in the following forms

$$E_{transmitted}(x_1, x_3 > 0) = A_t^q[-\eta + 2cos(q_{SL}x_1)\,]e^{-q_{SL}x_3} + A_t^{ik}[1 + \eta cos(q_{SL}x_1)\,]e^{-ikx_3} \quad \text{(S13)}$$

$$E_{backscattered}(x_1, x_3) = A_s^{-q}[-\eta + 2cos(q_{SL}x_1)\,]e^{q_{SL}x_3} + A_s^{-ik}[1 + \eta cos(q_{SL}x_1)\,]e^{ikx_3}. \quad \text{(S14)}$$

In the single scattering approximation, valid due to the smallness of the acoustic strain, it is possible, first, while neglecting the acoustically scattered field, to find (from the conditions of the continuity at the interface of the electrical field component E_2 and of the magnetic field component $H_1 \sim \partial E_2/\partial x_3$) the reflection/transmission coefficients, defining the amplitudes of the reflected/transmitted probe fields

$$r \equiv \frac{\langle E_r\rangle}{E_i} \cong -\frac{n-1}{n+1},\ t_{\frac{air}{SL}} \equiv \frac{A_t^{ik}}{E_i} \cong \frac{2}{n+1},\ \frac{A_t^q}{E_i} \cong -\frac{\eta}{n+1}\frac{\left(n+\sqrt{1-\frac{\lambda_0^2}{d_{SL}^2{}^2}}\right)}{\left(\sqrt{n^2-\frac{\lambda_0^2}{d_{SL}^2{}^2}}+\sqrt{1-\frac{\lambda_0^2}{d_{SL}^2{}^2}}\right)} \approx -\frac{1}{2(n+1)}\eta \ll 1. \quad \text{(S15)}$$

The solutions in Eq. (S15), where only the leading order terms in the powers of the small parameter $\eta << 1$ has been retained, indicate the smallness of the probe optical field transmitted in the first diffraction order, i.e., of the evanescent part of the transmitted field, and the direct relation of this smallness to the sub-optical periodicity of the SL.

The weakness of the coupling between the different diffraction orders (when light is transmitted across the air/SL interface in the considered sub-optical SL) revealed by Eq. (S15) suggests that, if the detection process is possible in the asymptotic case $\eta = 0$, then accounting for the corrections of its description in the case $\eta \neq 0, \eta \ll 1$ would be unnecessary. In the limit $\eta = 0$, the transmitted light field in Eq. (S13) reduces to $E_{transmitted}(x_1, x_3 > 0, \eta = 0) = A_t^{ik}e^{-ikx_3}$ and only the plane unmodulated acoustically backscattered field, i.e., in the zeroth diffraction order in Eq. (S14), can contribute (after the transmission from the SL into air) to the signal of our interest, $E_{backscattered}(x_1, x_3 > 0, \eta = 0) = A_s^{-ik}e^{ikx_3}$. These light fields are coupled due to the acoustic field in the following Helmholtz equation

$$\left(\frac{\partial^2}{\partial x_1^2} + \frac{\partial^2}{\partial x_3^2}\right)E + k_0^2[\varepsilon(x_1) + \varepsilon_{acoust}(x_1, x_3)]E = 0,$$

where $\varepsilon_{acoust}(x_1, x_3 > 0)$ denotes acoustically induced changes in the relative permittivity. In the single scattering approximation, this equation describes the emission of the scattered probe light by the acoustically-induced non-linear polarization:

$$\frac{\partial^2}{\partial x_3^2}E_s + k_0^2\langle\varepsilon\rangle E_s = -k_0^2\langle\varepsilon_{acoust}(x_1,x_3)\rangle E_{transmitted}. \quad \text{(S16)}$$

Here the lateral averaging over the period of the SL takes into account the fact that the plane (laterally unmodulated) transmitted probe light field E_t can be scattered into the plane (laterally unmodulated) light only by the laterally unmodulated (averaged) component of the acoustically induced changes of permittivity. Note that Eq. (S16) accounts for both forward and backward propagating scattered light but only the evaluation of the backward scattered probe light incident on SL/air interface is required for the evaluation of the signal. The required solution of Eq. (S16) leads, finally, to the following presentation for the amplitude of the acoustically scattered probe light contributing to the changes in the transient optical reflectivity monitored by the photodetector (Fig. S3)

$$\Delta r = -\frac{ik}{2}(1-r^2)\int_0^\infty \frac{\langle\varepsilon_{acoust}(x_1,x_3)\rangle}{\langle\varepsilon\rangle} e^{-2ikx_3}dx_3. \quad \text{(S17)}$$

If we introduce the notation δf for the acoustically induced variation of the physical parameter f and assume that the SLs for the generation and the detection of SAW are identical (as it is in our experiments), then, in the gR SAW, Eq. (S8), acting on the electrical permittivity, Eq. (S10), $\langle\varepsilon_{acoust}(x_1,x_3)\rangle$ can be written as

$$\langle\varepsilon_{acoust}(x_1,x_3)\rangle \equiv \langle\delta\boldsymbol{\varepsilon}(x_1,x_3)\rangle = \langle\delta\langle\varepsilon\rangle + 2\delta(\Delta\varepsilon)\cos(q_{SL}x_1)\rangle.$$

The first term in this expression describes the possibility to detect generalized Rayleigh SAWs due to the fact that its spatially unmodulated component modulates in time the spatially-averaged part of the SL electrical permittivity. The second term predicts the possibility to detect generalized Rayleigh SAWs due to the interaction (parametric) of the spatially modulated ($\sim\cos(qx_1)$) component of SAWs with the spatially modulated part of the electrical permittivity.

An intermediate result, which is obtained with the use of Eq. (S10) for the SL with the equal thicknesses of two layers, $d^{(1)} = d^{(2)}$ reads

$$\langle\varepsilon_{acoust}(x_1,x_3)\rangle = \left(\varepsilon^{(1)}-\varepsilon^{(2)}\right)\frac{\delta d^{(1)}-\delta d^{(2)}}{2d_{SL}} + \langle\frac{\delta\varepsilon^{(1)}+\delta\varepsilon^{(2)}}{2} + 2\frac{\delta\varepsilon^{(1)}-\delta\varepsilon^{(2)}}{\pi}\cos(q_{SL}x_1)\rangle. \quad \text{(S18)}$$

Here the terms $\sim(\delta d^{(1)}-\delta d^{(2)})$ and $\sim(\delta\varepsilon^{(1)}+\delta\varepsilon^{(2)})$ are contributions from $\langle\delta\langle\varepsilon\rangle\rangle$. Equation (S18) attracts our attention to the fact that acousto-optic detection of SAWs, even in the SLs with constant period, which is not modified by the symmetric generalized Rayleigh SAW under consideration here and $\delta d^{(1)}+\delta d^{(2)} = 0$, could take place not only due to the photo-elastic effect in the individual layers. If $\varepsilon^{(1)} \neq \varepsilon^{(2)}$, the detection can be also due to the geometrical effect of the acoustically induced variations in the thicknesses of the layers. For the SAW in Eq. (S8), this geometrical contribution can be evaluated as follows

$$\frac{\langle\varepsilon_{acoust}(x_1,x_3)\rangle_{geom}}{\left(\varepsilon^{(1)}-\varepsilon^{(2)}\right)} = \frac{\delta d^{(1)}}{d_{SL}} = \frac{u_1\left(x_1=\frac{d_{SL}}{4},x_3\right)-u_1\left(x_1=-\frac{d_{SL}}{4},x_3\right)}{d_{SL}} = \frac{2u_1\left(x_1=\frac{d_{SL}}{4},x_3\right)}{d_{SL}} = \frac{4}{d_{SL}}\sum_{j=L,T}A_j e^{-\alpha_j x_3}. \quad \text{(S19)}$$

The derivation of Eq. (S19) assumes that only the horizontal components of the mechanical displacement in SAWs contribute to the modification (breathing) of the layers thicknesses. The contributions into $\langle\varepsilon_{acoust}(x_3)\rangle$ from the photo-elastic effect in the individual layers are described by

$$\begin{aligned}\delta\varepsilon^{(i)} &= -(\varepsilon^{(i)})^2 p_{21}^{(i)}\left(\frac{\partial u_1}{\partial x_1}+\frac{\partial u_3}{\partial x_3}\right) \equiv \bar{p}^{(i)}\left(\frac{\partial u_1}{\partial x_1}+\frac{\partial u_3}{\partial x_3}\right)\\ &= \bar{p}^{(i)}\sum_{j=L,T}A_j\left\{-\alpha_j\left(\frac{u_0}{u_S}\right)_j + 2\left[q-\alpha_j\left(\frac{u_C}{u_S}\right)_j\right]cos(q_{SL}x_1)\right\}e^{-\alpha_j x_3}.\end{aligned}$$

Here $p_{21}^{(i)}$ denote the relevant component of the photo-elastic tensor [S7]. Substitution of this result into Eq. (S18) and averaging over the SL period lead to the description of photo-elastic contribution into $\langle \varepsilon_{acoust}(x_1, x_3) \rangle$

$$\langle \varepsilon_{acoust}(x_3) \rangle_{photo-elastic} = \sum_{j=L,T} A_j \left\{ -\alpha_j \left(\frac{u_0}{u_S}\right)_j \frac{\bar{p}^{(1)}+\bar{p}^{(2)}}{2} + 2\left[q - \alpha_j \left(\frac{u_C}{u_S}\right)_j \right] \frac{\bar{p}^{(1)}-\bar{p}^{(2)}}{\pi} \right\} e^{-\alpha_j x_3}. \quad \text{(S20)}$$

The first combination in the figure brackets of Eq. (S20) predicts the detection due to the SL averaged photo-elasticity, $\frac{\bar{p}^{(1)}+\bar{p}^{(2)}}{2}$, of the laterally unmodulated (averaged) component of the generalized Rayleigh wave, $\sim \left(\frac{u_0}{u_S}\right)_j \sim \mu$ (see Eqs. (S7) and (S8)). The second combination in the figure brackets of Eq. (S20), is due to the averaging of the product of the laterally modulated components of the strain in SAW and laterally modulated component of the SL photo-elasticity. It appears due to $\langle cos^2(q_{SL} x_1) \rangle = 1/2 \neq 0$ and predicts the changes in the averaged acousto-optical response of the SL due to the coupling of the SL periodicity to the laterally modulated components of the SAW. It is worth mentioning here that we call Eq. (S20) the photo-elastic contribution, because it would disappear with diminishing components of the photo-elastic tensor $p_{21}^{(i)}$, however the parameter controlling this contribution, i.e., $\bar{p}^{(i)}$, is additionally proportional to the square of the permittivity, $\bar{p}^{(i)} \equiv -(\varepsilon^{(i)})^2 p_{21}^{(i)}$.

The results in Eqs. (S19) and (S20) demonstrate that even when $d_{SL}/\lambda \to 0$, i.e., in deeply sub-optical SLs, the detection of deeply sub-optical generalized Rayleigh SAWs is possible. It is theoretically possible even in the absence of the contrast between both the permittivity and photo-elastic constants of the individual layers. In this case, the SAW is detected via its laterally unmodulated component, which is an essential feature of the generalized Rayleigh waves in the considered nanostructured sample. However, in the case of weak contrast between both the densities and the elastic moduli of the individual layers, i.e., in the regime $\mu \ll 1$ evaluated in details in Supplementary 1, the dominant contributions to the detection of SAWs are expected due to the contrast in either permittivity, or photo-elastic constant, or both, of the individual layers. This contrast has not been assumed a weak one in the above-presented theoretical approach. Moreover, for the effective generation of SAWs by the pump laser pulses, the optical contrast between the individual layers is profitable to increase, e. g., combining the layers opaque and transparent to pump light. Thus, in the limiting case, where both $\mu \to 0$ and $d_{SL}/\lambda \to 0$, the acoustically-induced changes in electric field reflectivity are described by:

$$\frac{\Delta r}{r} = \frac{4ik}{(\varepsilon^{(1)}+\varepsilon^{(2)})}\left(r - \frac{1}{r}\right) \sum_{j=L,T} \frac{A_j}{\alpha_j + 2ik} \left\{ \left(\varepsilon^{(1)} - \varepsilon^{(2)}\right) + \left[1 - \frac{d_{SL}\alpha_j}{2\pi} \left(\frac{u_C}{u_S}\right)_j \right] \left(\bar{p}^{(1)} - \bar{p}^{(2)}\right) \right\}. \quad \text{(S21)}$$

This solution is obtained by substitution of Eqs. (S19) and (S20) in Eq. (S17). If we take into account that the penetration depths of the gR SAW components are of the order of the SAW wavelength, i.e., $\alpha_j \sim 1/d_{SL}$, then, in the considered limit $d/\lambda \to 0$, Eq. (S21) additionally simplifies to

$$\frac{\Delta r}{r} = \frac{4ik}{(\varepsilon^{(1)}+\varepsilon^{(2)})}\left(r - \frac{1}{r}\right) \sum_{j=L,T} \frac{A_j}{\alpha_j} \left\{ \left(\varepsilon^{(1)} - \varepsilon^{(2)}\right) + \left[1 - \frac{d_{SL}\alpha_j}{2\pi} \left(\frac{u_C}{u_S}\right)_j \right] \left(\bar{p}^{(1)} - \bar{p}^{(2)}\right) \right\}, \quad \text{(S22)}$$

demonstrating that $\Delta r/r \sim d_{SL}/\lambda$. Thus, the SAW induced transient reflectivity signal inevitably diminishes with the diminishing pitch of the SL even in its leading order retained in Eq. (S22). However, this diminishing is much slower than in some other processes of light scattering by sub-optical inhomogeneities/objects. For example, the Rayleigh scattering of light by sub-optical spheres

scales $\sim(d_{SL}/\lambda)^4$. Moreover, it is important to mention here that to reach the regime, which we denote for the simplicity of the above discussions as $d_{SL}/\lambda \to 0$, could be not that easy under some practical circumstances. In fact, the precise condition for the transition from Eq. (S21) to Eq. (S22) is not $d/\lambda \ll 1$, but $4\pi|n|d_{SL}/\lambda_0 \ll 1$, where $|n|$ denotes the modulus of the averaged refractive index of the SL for the probe light of the wavelength λ_0 in vacuum. In the considered SL with the equal thicknesses of the individual layers, even if one of the two different layers strongly absorbs or reflects probe light, then $\frac{\lambda_0}{4\pi|n|} \approx 20-30$ nm. In this case, the asymptotic $\Delta r/r \sim d_{SL}/\lambda$ could be reached only in the SLs with the single digit nanometers period.

To conclude, it is worth reminding here that in our optical scheme only the amplitude of $\Delta r/r$ and not its phase is monitored. The signal in this optical scheme is due to the changes in the light intensity reflectivity, $R \equiv rr^*$, $dR/R \equiv 2Re(\Delta r/r)$ [S8], where "*" denotes the complex conjugation. This is one of the reasons for omitting, in the above-presented theory, the contribution to the detection process of SAWs from the motion of the air/SL interface induced by them [S9]. In fact, in analogy with the above-presented theoretical analysis, one could expect that the generalized Rayleigh SAW, in addition to lateral surface ripples, could induce the average surface displacement. However, this averaged surface displacement modifies only the phase and not the amplitude of $\Delta r/r$. This averaged surface motion could be monitored by the optical interferometry or by the beam deflection technique, if required. At the same time the SAW induced ripples with the sub-optical periodicity are diffracting the incident probe light into the evanescent orders (see the second term in Eq. (S11)), where it does not reach the photodetector.

[S6] Botti, S., & Andreani, L. C. (2001). Electronic states and optical properties of GaAs/AlAs and GaAs/vacuum superlattices by the linear combination of bulk bands method. *Physical Review B*, *63*(23), 235313.

[S7] Nye, J. F. (1985). *Physical properties of crystals: their representation by tensors and matrices*. Oxford university press.

[S8] Thomsen, C., Grahn, H. T., Maris, H. J., & Tauc, J. (1986). Surface generation and detection of phonons by picosecond light pulses. *Physical Review B*, *34*(6), 4129.

[S9] Loudon, R. (1978). Theory of surface-ripple Brillouin scattering by solids. *Physical Review Letters*, *40*(9), 581